Scaling of Magnetically Levitated Homopolar Hollow-Shaft Machines

C. Zingerli,
I. Coray,
J. Weber,
T. Nussbaumer,
J. W. Kolar

Scaling of Magnetically Levitated Homopolar Hollow-Shaft Machines

Claudius M. Zingerli[1], Ivan Coray[1], Jonathan Weber[1], Thomas Nussbaumer[2], Johann W. Kolar[1]

1: Power Electronic Systems Laboratory, ETH Zurich, CH - 8092 Zurich

2: Levitronix GmbH, Technoparkstr. 1, CH - 8005 Zurich

Abstract—In this paper, we analyze scaling issues that arise when the size of a magnetically levitated hollow-shaft machine is varied, but the output power is kept constant. Reducing the size by a factor of two leads to a required increase in speed by a factor of about three. Because the losses of previously used topologies did not scale well we suggest and analyze a different topology: the combined homopolar magnetic bearing (CHB). The proposed design methodology has been experimentally verified in a prototype product.

Index Terms—Magnetic levitation, Modeling, Eddy currents, Permanent magnet machines, Bearingless drives, Scaling

I. MOTIVATION

In the last thirty years, magnetic bearings have become more and more common. Due to comparably low force density[1], high complexity, delicate control and usually higher costs, uses are found mainly in applications that were not possible with mechanical bearings or merely with comparably high efforts. Such applications include machines operating at very high rotational speeds [2–4], or handling media that are very aggressive or sensitive to contamination [5].

Moreover, such applications can often be found in areas where space or weight is limited or expensive like aerospace [6], clean rooms [7] or body mounted systems [5]. It is therefore advantageous to minimize the size of such a machine.

Our subject of research is the magnetically levitated axial pump. Several different topologies of such machines were compared in [8]. Although - the magnetically levitated homopolar hollow shaft machine (MHM, [9]) topology was predicted to show minimal losses due to the small amplitude of the magnetic flux density in the rotor, its losses are still a challenge at higher speeds. In a previous study [10], the suitability of a MHM as shown in Figure 2a) has been analyzed. It is definitively suitable for the specifications given there, but we want to shrink the size of the machine by a factor of two while keeping the output power constant.

While the magnetic circuits of the drive and bearing on the stator side were already separated in [10], in the topology we propose, the magnetic circuits of the drive and bearing on the rotor side are separated as well. To keep the machine flat, the drive is placed in the hub of the machine using a permanent magnet synchronous machine (PMSM).

In the next chapters, we explain the choice of topology, analyze several design aspects, model losses, ending up with a prototype system as shown in Figure 1.
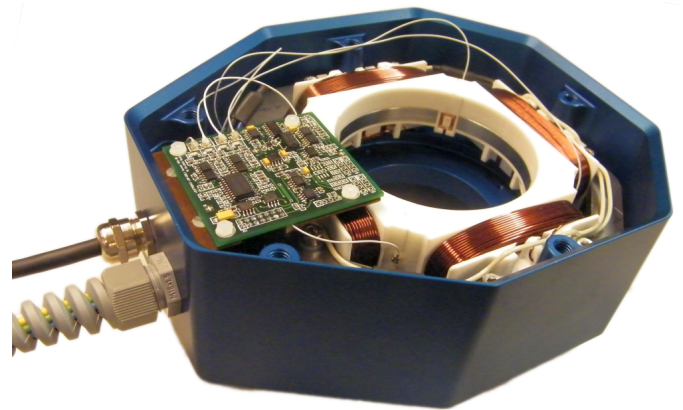

Figure 1: Prototype of a high-speed magnetically levitated hollow-shaft PMSM.

II. TOPOLOGY

For pump applications, the following affinity laws relate volume flow, pressure and power of similar machines:

$$\frac{Q_1}{Q_2} = \left(\frac{D_1}{D_2}\right)^3 \cdot \left(\frac{N_1}{N_2}\right) \quad \text{Volume flow} \quad (1)$$

$$\frac{Y_1}{Y_2} = \left(\frac{D_1}{D_2}\right)^2 \cdot \left(\frac{N_1}{N_2}\right)^2 \quad \text{Pressure} \quad (2)$$

$$\frac{P_1}{P_2} = \left(\frac{D_1}{D_2}\right)^5 \cdot \left(\frac{N_1}{N_2}\right)^3 \quad \text{Power} \quad (3)$$

If the effective rotor diameter is reduced from $D_1 = 130\,\text{mm}$

(as in [10]) to $D_2 = 68\,\text{mm}$, which is approximately $D_2 = \frac{1}{2} \cdot D_1$, the rotational speed of the machine has to be increased from $N_1 = 10\,\text{krpm}$ to the values shown in Table I.

Table I: Resulting speeds using pump affinity laws for a reduced diameter ($D_2 = \frac{1}{2} \cdot D_1$).

| n/krpm	Q_2/Q_1	Y_2/Y_1	P_2/P_1	U
10	$1/8$	$1/4$	0.0313	45 m/s
20	$1/4$	1	0.25	90 m/s
32	0.4	2.5	1	144 m/s
50	$5/8$	6.25	3.9	225 m/s
80	1	16	16	360 m/s

For a constant output power ($P_2 = P_1$), speed must be increased to $N_2 = 32\,\text{krpm}$. For a constant volume flow ($Q_2 = Q_1$), speed must be increased to $N_2 = 80\,\text{krpm}$ where the circumferential speed U is above the speed of sound under STP conditions; this case has not been studied further.

The topology choice focuses on small machine volume and low losses. We started with MHM, shown in Figure 2a. Since the major parts of the MHM losses scale at least with ω^2, maintaining this topology makes cooling difficult because of the fact that most losses occur in the rotor. If the drive cores are rotated (Figure 2b), the number of rotor poles can be reduced resulting in a lower electrical frequency while losing the independence of the bearing force from the rotor angle. A similar approach was proposed in [11] - the drive and bearing circuits were placed at different axial positions, leading to lower coupling, however increasing the axial length and hence the volume of the machine.

Even if all the topologies mentioned above allow for a free hub design, it is still difficult to benefit from this liberty of design. Regarding fluid transport, the hub section is of low importance, easily to be drawn from the affinity laws (1)-(3). That's why we moved the drive to the hub by placing a sensorless controlled external rotor PMSM in it. The number of magnets on the bearing rotor and stator has been doubled to produce a constant magnetic field all around the rotor. Freed from the need of discrete bearing stator pole widths (as opposed to the MHM topology), we formed the poles as wide as possible to minimize the change of magnetic reluctance around the rotor. A smaller amplitude of the magnetic reluctance leads to smaller changes in the magnetic flux density in the rotor parts, and accordingly to smaller eddy current losses. An upper limit for the stator pole width is needed to allow the placement of position sensors for the rotor.

We call this topology a combined homopolar bearing (CHB) owing to the combination of an active two-axis radial magnetic bearing with a passive three-axis axial and tilt magnetic bearing in a homopolar configuration. A model of the CHB is shown in Figure 3.

Any of the presented topologies can be configured in both an asymmetric (as shown in Figures 2 and 3) or symmetric way. In a symmetric configuration, permanent magnets are placed on both sides of the rotor and/or stator. A symmetric configuration highly increases stiffness, but also size, weight and eddy current losses as experienced using the machine from [10].
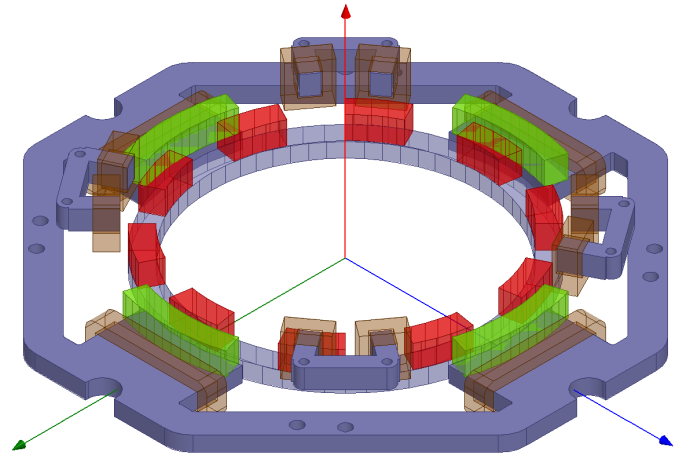
(a) Scaled model of the MHM topology.
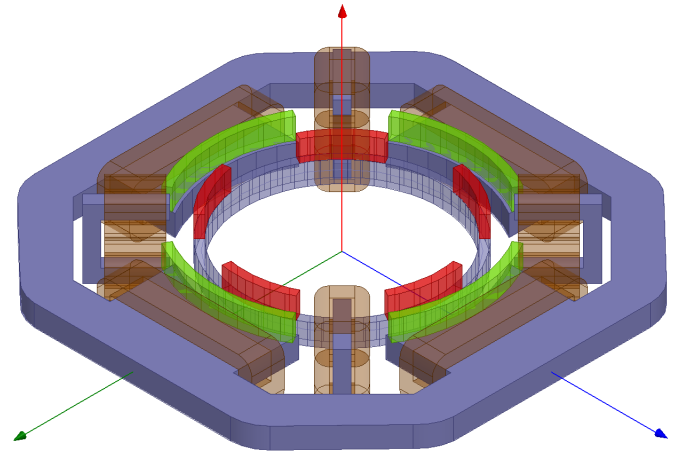
(b) MHM topology with rotated drive cores allows for a reduced number of rotor poles.

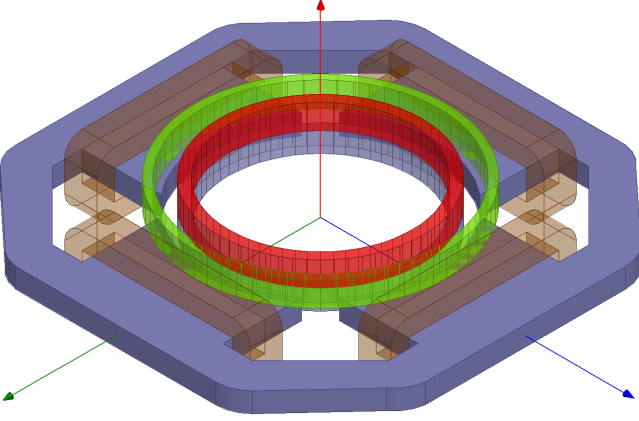Figure 2: Two studied variants of the MHM topology.

Figure 3: Combined homopolar bearing (CHB) topology with drive in the hub (not shown). The red and green rings are axially magnetized permanent magnets on the rotor and stator that - together with the iron (purple) create the passive magnetic axial and tilt bearing. The coils around the stator iron poles are used to control the radial position of the rotor.

III. DESIGN

The key parameters of the system are given in Table II.

Table II: Key parameters of the experimental system

Rotor outer diameter d_o	86 mm
Rotor mass m_r	0.3 kg
Rotor height h_r	25 mm
Rotor design speed n_{max}	32000 $1/\text{min}$
Rotor circumferal speed U	144 m/s
Mechanic air gap δ_{mech}	1.5 mm
Magnetic air gap δ_{mag}	5 mm
Active bearing axes p_{BNG}	2
Passive tilting stiffness k_a	-0.16 Nm/°
Passive axial stiffness k_z	-10.5 N/mm
Passive radial stiffness k_x	10.7 N/mm
Current-Force constant k_i	37 mN/A/turn
Bearing induction index A_L	325 nH/turn^2

A. Magnetic Design

Due to the complexity of the magnetic flux pathes and there being wide air gaps causing major parts of the flux go through stray pathes, the magnetic circuit was not designed analytically - but directly using a 3D finite element method (FEM) based simulation. This means, based on previous design experiences and by performing a parameter sensitivity analysis, which, today, can be regarded as very efficient thanks to increasing computer power.

Our objectives were high stiffness, compact size and little material on the rotor granting much space for the passing fluid.

A critical design aspect of the radial active magnetic bearing is that it must gain enough force to lift the rotor (this results in a lower limit on number of ampere-turns) yet has to be dynamic enough to stably levitate the rotor (this results in an upper limit on number of turns and a lower limit on voltage). Using the methodology from [12] and choosing $N = 100$ turns, the mechanical and electrical time constants

$$\tau_{\text{mech}} \approx \sqrt{\frac{m_r}{k_y}} = 5.3 \, \text{ms} \tag{4}$$

$$\tau_{\text{el}} \approx \frac{I \cdot A_L \cdot N^2}{V} = 680 \, \mu s \tag{5}$$

and therefore

$$\tau_{\text{mech}} > 5 \cdot \tau_{\text{el}} \tag{6}$$

which allows for sufficient stability margin for the bearing controller supplying $V = 24$ V and $I = 5$ A to the coils.

Further, the possibility has been studied of realizing a symmetric configuration with permanent magnets on both sides of the rotor and/or stator. While both - asymmetric and symmetric configurations - have been successfully tested in later experiments, the symmetric configuration proved to be less susceptible to tilting and axial oscillations than the asymmetric configuration.

B. Mechanical Design

The design process follows a similar path as proposed in [10]. The centrifugal loads in the rotor in this design are significantly higher. The tension σ'_{sh} in the (thin) rotor shell resulting from rotation with an angular frequency ω can be calculated using Barlow's formula to $\sigma'_{sh} = \rho \cdot r \cdot \omega^2$ at the shell radius r and density ρ. We assume that the rotor's magnets also hit onto the shell, so the tension increases to

$$\sigma_{sh} = \omega^2 \cdot \left(\rho_{sh} \cdot r_{sh}^2 + \rho_{mag} \cdot r_{sh} \cdot r_{mag} \cdot \frac{d_{mag}}{d_{sh}} \right) \tag{7}$$

with ρ_{sh}, ρ_{mag} the specific weights of the rotor shell and magnets, r_{sh}, r_{mag} the radii and d_{sh}, d_{mag} radial thicknesses. This gives a tension of $\sigma_{sh} = 260$ MPa at a speed of $n = 32$ krpm in the $d_{sh} = 2$ mm thick shell which provides some safety margin for stainless steel 1.4301.

IV. LOSSES

A. Electrical

Electrical losses in the machine consist of ohmic, eddy current and hysteresis losses. The latter are assumed to be small as little ferromagnetic material sees changing fluxes. Further, losses of the motor and drive are not covered in this study.

Bearing copper losses are inherently small since when placing the machine horizontally only rotor imbalance forces have to be considered - which are in the range under $1\,\text{Arms}$. Therefore they won't play a major role.

Eddy currents in the rotor shell constitute the dominant source of losses in the MHM topology. Therefore a detailed analysis of this source of losses was performed for the CHB topology as well.

To make a qualitative comparison, the flux density in the rotor shell was calculated for both topologies using their magnetostatic FEM models. Figure 4 shows the results using probes in the rotor shell at the upper limit of the rotor magnets (top curves), center of the rotor (middle curves) and below the rotor back iron (bottom curves). While the mean values are comparable in both topologies, the amplitude in the MHM topology is much higher. Clearly visible are the bearing poles in all curves ($90\,°$ periodicity) and the drive poles in the MHM topology ($18\,°$ periodicity). This changing flux density in the (conducting) rotor shell leads to eddy current losses.

As the qualitative analysis predicts a big improvement by this topological change, a quantitative analysis was performed as well. In this analysis, losses were studied using transient moving-mesh FEM-based simulations as shown in Figure 5. Current eddies are predicted in the rotor shell at the edges of the bearing stator. Because the magnetic air gap between rotor and stator iron ($\delta_{\text{mag}} = 5\,\text{mm}$) is already in the range of the bearing pole separation, the flux density change is small and therefore also the amplitude of the flowing current. Losses in the range of $5\,\text{W} - 10\,\text{W}$ are predicted. Despite the rotational symmetry of the rotor, the results of the model are not completely steady, so the precise value can be questioned.

While the quantitative analysis (magnetostatic simulations) took several minutes on a 16-core $2.4\,\text{GHz}$ PC, the qualitative analysis (transient simulation) at one fixed speed took more than 24h wall-clock time on the same machine. Iron laminations were modeled as electrically isolating and magnetically linear materials in order to speed up the simulation.
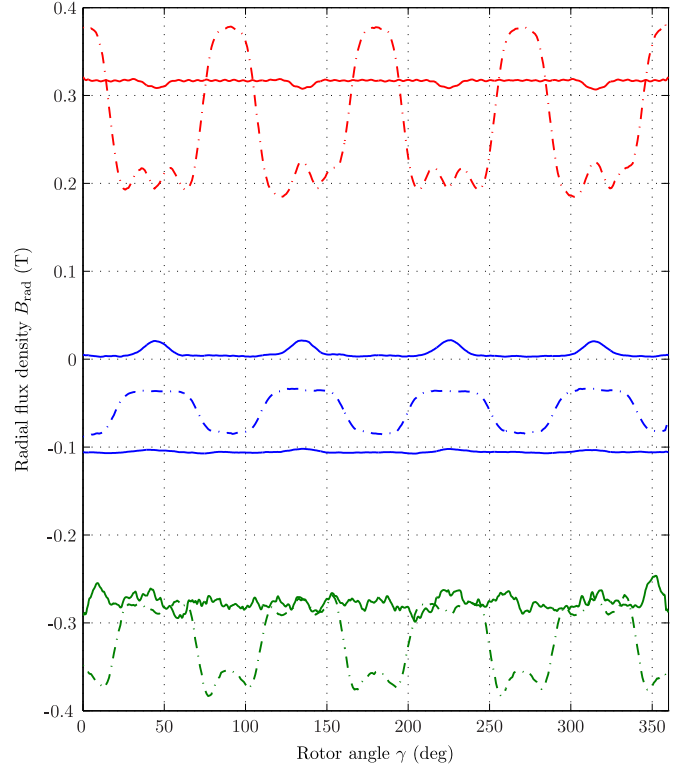
Figure 4: Radial flux density in the rotor shell calculated using a magnetostatic FEM model, shown at different axial positions (red: above rotor magents, blue: at Rotor center, green: below rotor). The amplitudes are greatly reduced from the MHM topology (dashed lines) to the CHB topology (solid lines) and therefore lower eddy current losses are predicted.

B. Windage

Due to the small gap and high differential speeds, high windage losses are expected in the gap between rotor and stator. The Taylor number

$$Ta \;=\; \frac{d_{\text{o}} \cdot \omega \cdot \delta_{\text{mech}}}{2 \cdot \nu} \cdot \sqrt{\frac{2 \cdot \delta_{\text{mech}}}{d_{\text{o}}}} \tag{8}$$

suggests that from a speed of $n = 30/\pi \cdot \omega = 5.6\,\text{krpm}$, a turbulent taylor flow develops in the air gap.

Using the friction coefficient c_f from [13], the friction power can be presumed as

$$c_f \;=\; 0.0325 \cdot \left(\frac{2 \cdot \delta_{\text{mech}}}{d_{\text{o}}}\right)^{0.3} \cdot Re^{-0.2} \tag{9}$$

$$P_{\text{air}} \;=\; c_f \cdot \omega^3 \cdot \rho \cdot \pi \cdot (d_{\text{o}}/2)^4 \cdot h \tag{10}$$

with the air density ρ, gap δ_{mech}, rotor height h and Reynolds number Re. At speeds of $n = 20\,\text{krpm}$ and $n = 32\,\text{krpm}$,
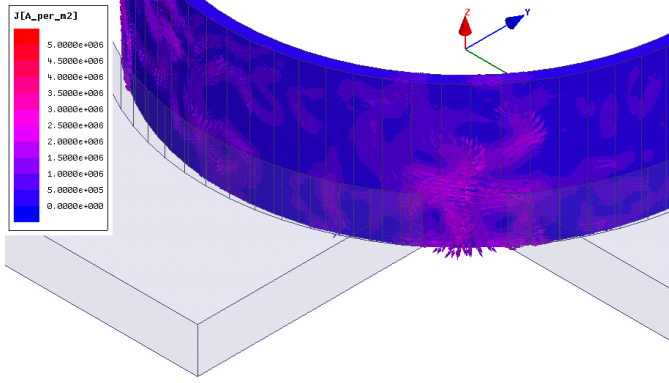
Figure 5: Eddy current density in the rotor shell (blue) using a transient FEM model. Current eddies (purple) can be seen at the edges of the bearing poles (gray blocks). The permanent magnets on the stator have been hidden for clarity.

$P_{\text{air}} = 6.3\,\text{W}$ and $P_{\text{air}} = 22.0\,\text{W}$ are lost in the cylindrical air gap if we assume hydraulically smooth surfaces.

V. RESULTS

The machine has been constructed and stable operation was achieved at any speed from zero up to $n = 28\,\text{krpm}$. Higher speeds were not tested fearing disintegration of the rotor.

To estimate the losses at high speeds, runoff experiments were performed, shown in Figure 6a. Performing a regression using

$$P_{\text{v,mod}} \quad = \quad c_0 \cdot \omega^2 + c_1 \cdot \omega^3 \qquad (11)$$

with $c_0 = 3.01\,\mu\text{J} \cdot \text{s}$ and $c_1 = 2.05\,\text{nJ} \cdot \text{s}^2$ as shown in Figure 6b leads to total losses of $P_{\text{v,mod}} = 47.0\,\text{W}$ at $n = 20\,\text{krpm}$ and predicted $P_{\text{v,mod}} = 111\,\text{W}$ at $n = 32\,\text{krpm}$.

In Figure 7, several runoff experiments are collected to give an estimation of the variation of the losses at higher speeds. The drive input power, marked with crosses at speeds $n = \{10\,\text{krpm},\ 16\,\text{krpm},\ 20\,\text{krpm},\ 25\,\text{krpm}\}$, is always higher than the measured losses since the drive was always disabled for measuring the loss.

Figure 7 and Table III clearly show that applying the MHM topology always produces higher losses than using the CHB topology at the same speed. If we compare the topologies with the same fluid power, the CHB topology presents less than half of the losses of the MHM topology. Except for a constant volume flow, downscaling the MHM based machine by a factor of two can easily be achieved with the improved CHB topology.
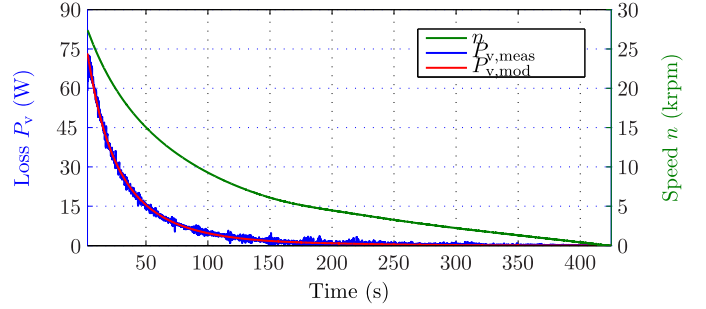
(a) Runoff experiment from 28 krpm (Green: Speed, Blue: Losses, Red: Modelled losses).
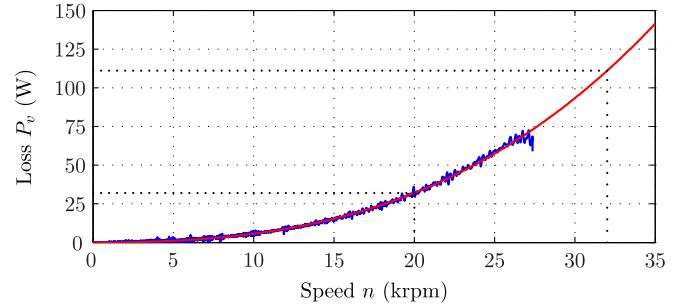
(b) Modeled system losses (red) based on measured data (blue).

Figure 6: Results from runoff experiment and accordingly modeled losses.

Table III: Comparison of the losses in the CHB topology ($D = 68\,\text{mm}$) and the MHM topology ($D = 130\,\text{mm}$).

Constant	n_{MHM}	n_{CHB}	Loss ratio CHB/MHM
Speed	7 krpm	7 krpm	5%
Fluid pressure	7 krpm	14 krpm	15%
Fluid power	7 krpm	22.4 krpm	42%

VI. CONCLUSIONS

The CHB topology allows increasing the speed of the motor which is absolutely essential to achieve a reduced system volume. Such a system has been successfully implemented and tested. Current results show that for the same hydraulic power, losses are less than half to those of the MHM topology, with the further advantage of a substantially reduced volume. Next steps involve upscaling the CHB topology to bigger radii to study dependence on topological choices and size.
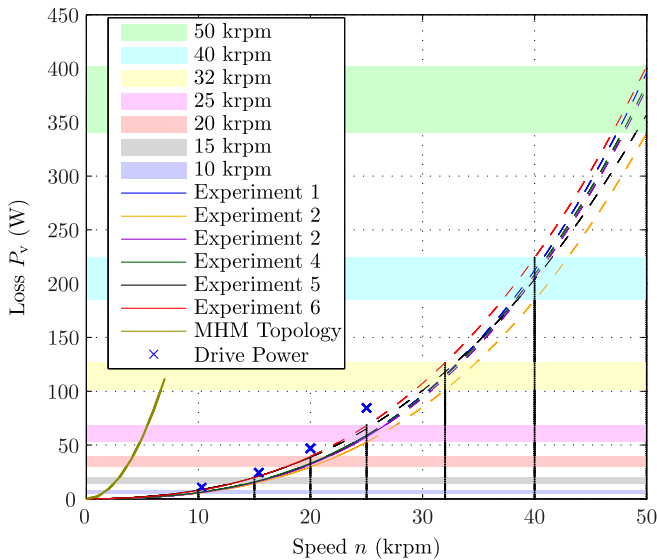
Figure 7: Comparison of several CHB runoff experiments with the existing MHM topology from [10] (olive) and CHB drive input power (crosses).

REFERENCES

[1] G. Schweitzer, "Active magnetic bearings chances and limitations," *Proc. 6th Internat. IFToMM Conf. on Rotor Dynamics*, 2002.

[2] C. Wildmann, T. Nussbaumer, and J. W. Kolar, "10 mrpm spinning ball motor: Preparing the next generation of ultra-high speed drive systems," in *Proc. Int. Power Electronics Conf. (IPEC)*, 2010, pp. 278–283.

[3] P. Imoberdorf, T. Nussbaumer, and J. W. Kolar, "Analysis of a combined radial-axial magnetic bearing for a high-speed drive system," in *Proc. th IET Int Power Electronics, Machines and Drives (PEMD 2010) Conf*, 2010, pp. 1–6.

[4] H. Mitterhofer and W. Amrhein, "Design aspects and test results of a high speed bearingless drive," in *Proc. IEEE Ninth Int Power Electronics and Drive Systems (PEDS) Conf*, 2011, pp. 705–710.

[5] R. S. Natale Barletta, "Design of a bearingless blood pump," *Third International Symposium on Magnetic Suspension Technology*, 1996.

[6] D. Krahenbuhl, C. Zwyssig, H. Weser, and J. W. Kolar, "A miniature, 500 000 rpm, electrically driven turbocompressor," in *Proc. IEEE Energy Conversion Congress and Exposition ECCE 2009*, 2009, pp. 3602–3608.

[7] T. Schneeberger, "Integriertes magnetisches lager- und antriebssystem fuer halbleiterwafer," Ph.D. dissertation, ETH Zurich, 2008.

[8] T. Nussbaumer, P. Karutz, F. Zurcher, and J. W. Kolar, "Magnetically levitated slice motors—an overview," *IEEE Trans. Ind. Appl.*, vol. 47, no. 2, pp. 754–766, 2011.

[9] T. Schneeberger, T. Nussbaumer, and J. W. Kolar, "Magnetically levitated homopolar hollow-shaft motor," *IEEE/ASME Trans. Mechatronics*, vol. 15, no. 1, pp. 97–107, 2010.

[10] C. M. Zingerli, J. W. Kolar, and T. Nussbaumer, "Analysis of rotor shell losses in a magnetically levitated homopolar hollow-shaft permanent magnet synchronous motor," in *Proc. 7th Int. Power Electronics and Motion Control Conf. (IPEMC)*, 2012.

[11] P. Karutz, "Magnetically levitated 2-level slice motor for application in high purity process environments," Ph.D. dissertation, ETH Zurich, 2010.

[12] T. Reichert, T. Nussbaumer, W. Gruber, and J. Kolar, "Bearingless permanent-magnet motor with 4/12 slot-pole ratio for bioreactor stirring applications," *Mechatronics, IEEE/ASME Transactions on*, vol. 16, no. 3, pp. 431 –439, june 2011.

[13] E. Bilgen and R. Boulos, "Functional dependence of torque coefficient of coaxial cylinders on gap width and reynolds numbers," *Journal of Fluids Engineering*, vol. 95, no. 1, pp. 122–126, 1973.